Effect of Flapping Frequency and Leading Edge Profile on Airfoil Leading Edge Vortical Structures

Wesley N. Fassmann
Brigham Young University

Scott L. Thomson
Brigham Young University

Abstract—**By varying leading edge geometry to wing profiles during flapping flight, Ozen and Rockwell observed a pattern of alternating spanwise vortices which minimized spanwise flow. As a follow up study to [1], this investigation explored the effect of flapping frequency on these previously observed streamwise vortical structures. By increasing the flapping frequency, the alternating streamwise vortices resulting from a sinusoidal leading edge became stretched in the path of the wing due to an increase of wing cross-radial velocity. The streamwise vortices are shown to minimize spanwise flow even after being stretched. Instabilities were formed at higher flapping frequencies ($f = 0.2$ Hz) due to velocity shear generated by the large cross-radial velocity. These instabilities began to break down the alternating streamwise vortices resulting in the development of a different flow structure including an increase of spanwise flow.**

Keywords—*flapping flight, sinusoidal leading edge, vortex generator, spanwise flow, streamwise vortex, passive flow control*

I. INTRODUCTION

With a greater understanding of the workings of the biological world, biomimetic designs are becoming increasingly popular in engineering. One area of particular interest is the use of unsteady flow features along the leading edge to augment force production, as seen along the flippers of humpback whales and wings of natural fliers.

Leading edge tubercles along the flipper of a humpback whale act as a passive streamwise vortex generator increasing force production at high angles of attack. By analyzing the morphology of humpback flippers, Fish and Battle [2] initially suggested that the presence of leading edge tubercles would act as vortex generators. Miklosovic et al. [3] used an idealized flipper model with and without a sinusoidal leading edge to quantify an increase of force production with a sinusoidal leading edge due to the development of streamwise vortices. Our previous study [4] used a digitized model of an adult humpback whale flipper to demonstrate a similar result with actual geometry. Hansen et al. [5] related the increase of force production due to a sinusoidal leading edge with more traditional vortex generators.

Flow visualization along idealized models has showed the development of streamwise vortices between tubercles. Using a 2D cross-section with a sinusoidal leading edge Custodio [6] studied the flow across an airfoil with and without tubercles using dye injection flow visualization at a Re ~ 1500. Custodio observed streamwise vortices supplying momentum to the boundary layer over the tubercles, resulting in a delay of separation.

By comparison, during flapping flight of many natural fliers, such as birds and insects, a spanwise vortex develops along the leading edge. This leading edge vortex augments lift as it remains attached, and once the leading edge separates it is swept downstream and contributes to the generation of a reverse Von Karman vortex street, resulting in added thrust. Using a flapping mechanism, Baik et al. [7] concluded that the circulation of this leading edge vortex is dependent on the reduced frequency (k), and minimally dependent on Strouhal number (St), but the resultant force generation is significantly dependent on St, but not k.

Passive vortex generators were initially identified in flapping flight on the wings of bats. Norberg [8] first suggested that the digits and arms projecting above the wing in addition to concentrations of hairs seemed to act as turbulence generators across the wings of bats. As a turbulence generator, these passive control devices would transition the flow from laminar to turbulent, preventing separation and minimizing the pressure drag. A follow-up study suggested that these leading edge control devices acted more similar to a vortex generator by maintaining lift and preventing stall at low speeds and high angles of attack [9].

By imaging two flat rectangular flapping wings, one with and without a sinusoidal leading edge, Ozen and Rockwell [1] investigated the resulting spanwise flow. They observed that the addition of a sinusoidal leading edge generated alternating streamwise vortices consistent with previous non-flapping investigations which minimized the spanwise flow present in flapping flight. They also determined that although a sinusoidal leading edge does influence the spanwise flow, the formation and size of the tip vortex seemed relatively unaffected. A follow up numerical simulation by Zhang et al. [10] used an airfoil section with a sinusoidal leading edge to determine the influence on force production for both gliding and flapping motions. This investigation demonstrated that a sinusoidal leading edge resulted in an improved performance during gliding with the possibilities of improvements for flapping flight.

Although the alternating streamwise vortices resulting from a sinusoidal leading edge minimizes spanwise flow along the leading edge where the LEV is formed, little is understood about how these vortices vary with flapping frequency. The intent of this investigation is to build upon the previous research of Ozen and Rockwell [1] and investigate the influence of different flapping frequencies on the development of leading edge streamwise vortices.

A. Initial Setup Comparison

Ozen and Rockwell [1] used a free-surface water tunnel with free stream velocity $U_\infty = 25.4$ mm/s, to observe the spanwise flow of a rectangular wing, one with a straight edge and the other with a sinusoidal-varying leading edge. The wing had a mean chord length (c) of 50.8 mm, thickness of 1.59 mm and half-span (b) of 101.6 mm. For the wing with a sinusoidal leading edge, the leading edge was defined as a sinusoid with $a/c = 0.098$ and $\lambda/c = 0.246$. With a pitching angle of 8° relative to the horizontal free stream velocity, the wing was oscillated at 0.047 Hz in a flapping motion by following a triangular trajectory with a maximum angle of 30°

By varying the flapping frequency of a similar experimental setup as Ozen and Rockwell [1] the influence of flapping frequency on the observed pattern of alternating vortices was determined. Table 1 compares the variations in parameters for the different flapping frequency cases and the parameters used by Ozen and Rockwell [1]. A flapping frequency of $f = 0.05$ Hz is the most comparable set to those parameters conducted by [1]. Even though the tested variations of the leading edge are comparable, the free stream velocity, half-span, and flapping frequency deviated slightly from the original study by [1].

Table 1: Experimental Parameters

Parameters	0.05 Hz	0.075 Hz	0.1 Hz	0.2 Hz	Ozen (0.047 Hz)
Free-stream Velocity (U_∞) [m/s]	23	23	23	23	25
Chord length (c) [mm]	50.8	50.8	50.8	50.8	50.8
Wing length (R) [mm]	101.6	101.6	101.6	101.6	95.25
Half-span length (b) [mm]	127	127	127	127	101.6
Wing thickness (t) [mm]	2	2	2	2	1.59
Sinusoidal amplitude (a/c)	0.10	0.10	0.10	0.10	0.098
Sinusoidal wavelength (λ/c)	0.25	0.25	0.25	0.25	0.246

In this study the two wing planforms, one with a straight and the other with a sinusoidal leading edge (see Fig. 2), were separately used. Each had a mean chord length of $c = 50.8$ mm, a wing length of $R = 101.6$ mm, and were 2 mm thick, which differed slightly from Ozen and Rockwell [1], see Table 1. The wing mount was 25.4 mm long, yielding a half-span of $b = 127$ mm. The leading edge sinusoids featured an amplitude of $a/c = 0.1$ and wavelength of $\lambda/c = 0.025$, comparable with those of Ozen and Rockwell [1], as seen in Figure 2.
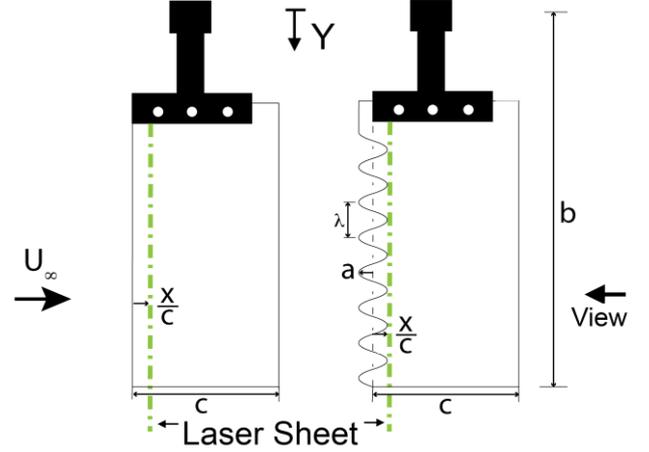
Figure 1: Wing planform designs demonstrating the straight and sinusoidal leading edges, in addition to the locations of the laser sheet and PIV camera view (illustration courtesy Keenan Eves).

B. Flapping Mechanism

The flapping mechanism previously developed at Brigham Young University [11] pictured in Figure 1, was used to perform the flapping kinematics. Motors connected to three shafts drove each wing with three independent rotational degrees of freedom (pitch, sweep, and deviation).

Figure 2: Flapping mechanism used for performing flapping kinematics with three independent rotational degrees of freedom including (pitch, sweep, and deviation).

C. Water Tunnel

This investigation was performed in a free-surface water tunnel, simulating a slow forward trajectory. The cross section at the test location was about 0.95 m wide and 0.46 m deep. PIV measurements were acquired at six different chordwise locations spaced from the centerline in the region of interest to determine the mean free stream velocity ($U_\infty = 23 \pm 3$ mm/s) and the maximum turbulence intensity level (< 3 %) in the area of interest. The flapping mechanism was placed in the middle of the measured volume, about 0.41 m from upstream honey comb and about 0.61 m from downstream honeycomb.

D. Wing Kinematics

The flapping wing kinematics was determined by the sweep motion (φ) and the pitch angle (θ). The vertical sweeping motion (φ), as illustrated in Fig. 4, was determined by a rounded triangular input (Equation [1]), while the pitching remained constant at $\theta = 8°$. A rounded triangular input was used to reduce wear on the mechanism hardware, even though Ozen and Rockwell [1] used a triangular input without the rounding at wing reversal.

$$\varphi = 30°\sin^{-1}[0.8221 \sin(2\pi f \, \text{time})] / [\sin^{-1}(0.8221)] \quad (1)$$
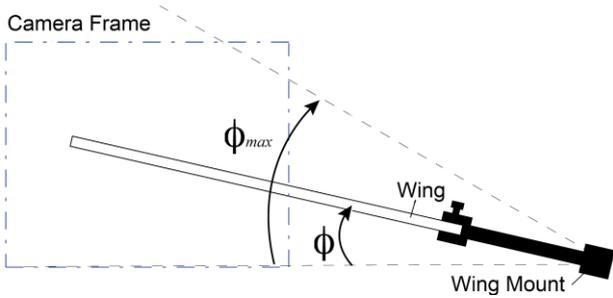
Figure 3: Wing and camera frame position. The dotted lines indicate the maximum wing sweep (φ_{max}), while the angle φ is the current wing position of the wing. The blue box indicates the relative position of the camera frame to the wing. Flow is out of the page (illustration courtesy Keenan Eves).

As previously described, the sweep kinematics (Equation 1) were dependent on the flapping frequency which varied from f = 0.2 Hz, 0.1 Hz, 0.075 Hz, and 0.05 Hz. Because the wing velocity, V_t, and effective angle of attack (α_e) of the wing are dependent on the flapping frequency, these were calculated for each flapping frequency according to Equations 2 and 3 used by [1], where $\alpha = 8°$ (the static angle of attack) and U_∞ is the free stream velocity. The calculated values are presented in Table 2.

$$V_t = 2\pi\varphi_{max}f \quad (2)$$

$$\alpha_e = \alpha_0 + \tan^{-1}(V_t/U_\infty) \quad (3)$$

Table 2: Comparison of current experimental parameters and reported parameters of [1] (left).

Flapping frequency (f) [Hz]	0.05	0.075	0.1	0.2	0.047
Wing velocity (V_t) [mm/s]	13.3	19.9	26.6	53.2	10.6
Effective angle of attack (α_e)	38°	48.9°	57.1°	74.6°	30.7°
Reynolds number (Re)	1170	1170	1170	1170	1300
Strouhal number (St)	0.29	0.43	0.69	1.38	0.22
Reduced frequency (k)	0.35	0.52	0.58	1.15	0.22

Variations in flapping frequency influenced the period but not the trajectory of wing kinematics. By changing the flapping frequency, the non-dimensional numbers which described flow characteristics were altered. Table 2 presents these non-dimensional parameters for each flapping frequency (f) and compares these parameters with those established by Ozen and Rockwell [1]. As the flapping frequency increased from 0.05 to 0.2 Hz, the Strouhal number (St) and reduced frequency (k) also increased from 0.29 and 0.35 to 1.38 and 1.15, respectively.

E. PIV Setup

Quantitative cross-flow velocity and vorticity measurements were acquired using a LaVision particle image velocimetry (PIV) system. The flow was seeded with 11 μm diameter hollow glass spheres (Potter Industries Inc., Sphericel 110P8). The LaVision PIV system included a double-pulsed Nd:YAG laser (532 nm) which generated an approximately 1.5 mm thick sheet across the wing at x/c = 0.11 as illustrated in Figures 2 and 4. A mirror was placed approximately 0.46 m downstream in order to reflect the spanwise image up to the mounted PIV camera, see Figure 5. The PIV camera was mounted with a Nikon 105 mm Nikkor lens. In order to synchronize the PIV system with the flapping mechanism, a TTL trigger was sent from the PIV system to the flapping mechanism to determine when to acquire images. The time delay between the camera images was changed depending on the flapping frequency and adjusted such that the mean pixel movement was between about 6-10 pixels in selected areas of interest. The PIV measurements were computed using a multi-pass cross-correlation with a decreasing window size from 64×64 pixels to 16×16 pixels with 50% overlap. Using ensemble phase averaging of 35 images, vorticity and velocity plots were generated. Spurious vectors of magnitude 1.2 times the RMS of the eight neighbor velocities were eliminated and replaced with the next highest correlation peak which met this criteria. As the PIV camera images through the water surface, the images were manually sorted to eliminate free surface effects. Subsequently, the vorticity (ω) was calculated as the curl of the resulting velocity.
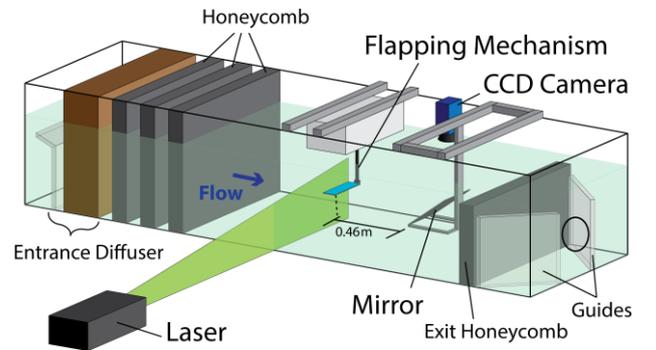
Figure 4: The PIV setup including a mirror placed downstream, the PIV camera mounted above the water tunnel to acquire reflected images, and the laser sheet (illustration courtesy Eric Tingey).

PIV data was acquired to characterize the influence of flapping frequency on the observed streamwise vortical structures. This data set focused on identifying the primary differences of vortical structures between a straight and sinusoidal leading edge at different flow domains. Using both the straight and sinusoidal leading edge, PIV images were acquired for each flapping frequency and wing at a phase angle of 13.3°, as was initially investigated by Ozen and Rockwell [1].

III. RESULTS

The streamwise vortical structures generated by both sinusoidal leading edge and straight leading edge were documented at different flapping frequencies. At low flapping frequency (f = 0.05 Hz) for a wing with a sinusoidal leading edge, a repetitive pattern of small scale alternating vortices were observed in the vicinity of the sinusoidal leading edge, as illustrated in Figure 4, similar to observations made by Ozen and Rockwell [1]. Because the half-span lengths differ between this investigation and Ozen and Rockwell, the first four alternating vortices (from right to left side) along the wing of this current study correlate to the last four alternating vortices from Ozen and Rockwell [1].

The non-dimensional vorticity magnitude and size of the vortices from this investigation appear to be comparable, even though there are slight discrepancies in the setup. By examining the development of these streamwise vortices of this current study along the tip, it appears that the vortices close to the wing tip begin to stretch upward due to the wing velocity to the wing (cross-radial velocity). The cross-radial velocity is the resulting velocity from sweeping motion of the wing. The previously described streamwise vortices appear to have a similar structure as the vortices observed by Custodio [2] at the leading edge of a stationary 2D airfoil with idealized tubercles at Re ~ 1500. As the flow passed on either side of the sinusoidal peaks, alternating vortices were developed (Fig. 4). The vortices observed at this lower frequency correspond to the respective locations of sinusoidal peaks along the leading edge of the wing.
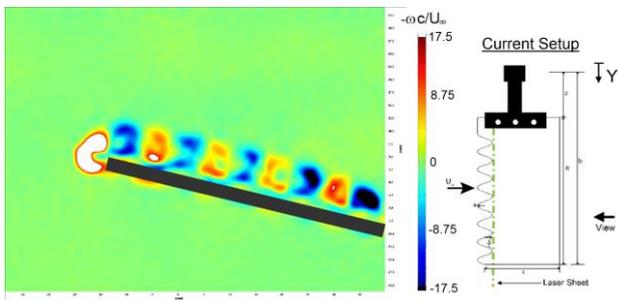
Figure 5: (right) Vorticity plot of a rectangular wing with a sinusoidal leading edge for f = 0.05 Hz and φ = 13.3°. Red arrows illustrate tubercle locations. Black line illustrates the wing.

With respect to a straight leading edge, a comparable vortex formation was observed in this study as reported by Ozen and Rockwell [1]. The plots of vorticity indicate the development of a spanwise flow (see Fig. 5). A positive and negative vortex is identified indicating the development of spanwise flow. Although the magnitude of vorticity is fairly similar for a sinusoidal leading edge between the current study and the reported data by Ozen and Rockwell [1], the vorticity magnitude of this study is significantly greater for a straight leading edge, potentially resulting in a much greater spanwise velocity (Fig. 5). A possible reason for this dramatic increase in spanwise flow is the increase of half-span length, although further investigation would be needed to determine influence of wing length to spanwise flow.

As the flapping frequency increases, the cross-radial velocity of the wing influences the development of the observed streamwise vortices. With respect to a straight leading edge at f = 0.05 Hz and 0.075 Hz (Figs. 7b, 7d, 8b, and 8d, on the last page), spanwise flow generates opposing vortices near the tip as in Fig. 6. As the flapping frequency increases from f = 0.05 Hz, the wing cross radial velocity contributes to the dissipation of this jet, resulting in a decrease of spanwise velocity (Fig. 7b, 7d, 7f, 8b, 8d, and 8f). At f = 0.2 Hz, the vorticies become significantly larger resulting in a much larger spanwise flow (Figs. 7h and 8h).

The magnitude of vorticity for the sinusoidal leading edge wing seemed to increase with increasing flapping frequency f (Figs. 7a, 7c, 7e, and 7g). This increase in magnitude could potentially result from an increase of flow past the sinusoidal peaks from the increase in cross-radial velocity. Although an increase in vorticity magnitude was observed due to the cross-radial velocity, the vorticity is stretched tangential to the wing (Figs. 7a, 7c, 7e, and 7g). Contrary to the wing with a straight leading edge, the spanwise flow increases with flapping frequency (Fig. 7). At f = 0.2 Hz, the alternating vorticites begin to break down near the tip, resulting in a significant increase of spanwise flow.
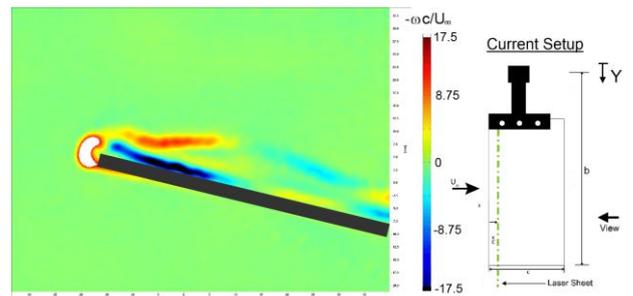
Figure 6: (right) Vorticity plot of a rectangular wing with a straight leading edge for f = 0.05 Hz and φ = 13.3°. Black line illustrates the wing

As the wing velocity increases with flapping frequency, Instabilities begin to form around the vortices. For higher frequencies such as f = 0.2 Hz, vortex instabilities cause the streamwise vortices to break down into smaller vortices. Vortical instabilities are developed due to a velocity shear in a continuous fluid and can lead to the transition to turbulence. Observations of this shearing of vortices can be seen as waviness on the edges of the streamwise vortices; see Figs. 7e,

7f, 7g, and 7h. The waviness increases with flapping frequency f, as would be expected due the flapping motion produces the velocity shear which would cause the instabilities to grow. At $f = 0.2$ Hz, the ordered pattern of alternating vortices has broken down between the peaks, but several large alternating vortices are observed in place of the usual pattern (Fig. 7g). Initial observations indicate that with the increase of flow velocity, instabilities have broken down the individual vortices at the peaks and generated these large alternating vortices. An evaluation of the calculated RMS shows that at higher flapping frequencies, the presence of instabilities plays an increased role in the disruption of vortices.

Even though the streamwise vortical structure varies with an increase of flapping frequency (f), an increase in flapping frequency had a limited effect on the passive spanwise control. With a straight leading edge, a y-direction (spanwise) flow is observed towards the tip at all frequencies tested. By comparing the sinusoidal leading edge, a decrease in y-direction velocity is observed (Fig. 8). A definite decrease in spanwise flow is observed at $f = 0.1$ Hz, due the relatively large tangential wing velocity, but by $f = 0.2$ Hz the spanwise flow has increased in magnitude. Even though a decrease is observed as a general trend, at flapping frequency of $f = 0.2$ Hz a significant spanwise velocity component is observed in the locations without the presence of alternating vortices. These observations indicate that even though the minimizing of spanwise velocity is observed through all of the flapping frequencies, the presence of a uniform alternating vortical structure developed by the sinusoidal leading edge has an increased significance on minimizing spanwise velocity.

Conclusion

By comparing two wing profiles, a straight and sinusoidal leading edge, at different flapping frequencies, the development of alternating vortices are further investigated. At a flapping frequency of $f = 0.05$ Hz, a similar vortical formation is observed for both a straight and sinusoidal leading edge as previously reported by [1]. A sinusoidal leading edge can be used to minimize spanwise flow by the generation of alternating streamwise vortices, but as flapping frequency increases these streamwise vortices being stretched in the path of the wing. Even after being elongated, these streamwise vortices minimize spanwise flow, until they begin to break down due to instabilities as seen at $f = 0.2$ Hz. These vortical instabilities are formed due to the presence of a velocity shear generated by the increase in flapping frequency and resulting cross-radial velocity.

An inspection of different phase angles indicates that alternating streamwise vortices result in a decrease of spanwise flow at different stroke angles. The development of alternating vortices are observed at $\varphi = 28°$. As the stroke progresses, separation between the wing and these alternating vortices are observed near the tip at flapping frequencies greater than f = 0.05 Hz. In addition to this separation between the wing, the generated vortices begin to break down with at the periphery with a flapping frequency of $f = 0.2$ Hz due to vortical instabilities resulting from the cross-radial velocity creating a velocity shear. Except for $f = 0.2$ Hz, spanwise flow is minimized at different flapping frequencies even with the vortices being separated from the wing..

REFERENCES

[1] Ozen, C. A., and D. Rockwell. "Control of vortical structures on a flapping wing via a sinusoidal leading-edge." Physics of Fluids (1994-present) 22.2 (2010): 021701.

[2] Fish, Franke E., and Juliann M. Battle. "Hydrodynamic design of the humpback whale flipper." Journal of Morphology 225.1 (1995): 51-60.

[3] Miklosovic, D. S., et al. "Leading-edge tubercles delay stall on humpback whale (Megaptera novaeangliae) flippers." Physics of Fluids (1994-present) 16.5 (2004): L39-L42.

[4] Fassmann, Wesley N., et al. "Hydrodynamics of a Digitized Adult Humpback Whale Flipper." Bulletin of the American Physical Society 58 (2013).

[5] Hansen, Kristy L., Richard M. Kelso, and Bassam B. Dally. "Performance variations of leading-edge tubercles for distinct airfoil profiles." AIAA journal 49.1 (2011): 185-194.

[6] Custodio, Derrick. The effect of humpback whale-like leading edge protuberances on hydrofoil performance. Diss. Worcester Polytechnic Institute, 2007.Custodio

[7] Baik, Yeon Sik, et al. "Unsteady force generation and vortex dynamics of pitching and plunging aerofoils." Journal of Fluid Mechanics 709 (2012): 37-68.

[8] Norberg, R., A. Fagraeus, and K. Lidman. "Reaction of human smooth muscle antibody with human platelets." Clinical and experimental immunology 21.2 (1975): 284.

[9] Norberg, Ulla M. "Vertebrate flight: mechanics, physiology, morphology, ecology and evolution." (1990).

[10] Zhang, Xingwei, et al. "Numerical study on effect of leading-edge tubercles." Aircraft Engineering and Aerospace Technology 85.4 (2013): 1-1.

[11] George, Ryan B., et al. "A Differentially Driven Flapping Wing Mechanism for Force Analysis and Trajectory Optimization." International Journal of Micro Air Vehicles 4.1 (2012): 31-50.
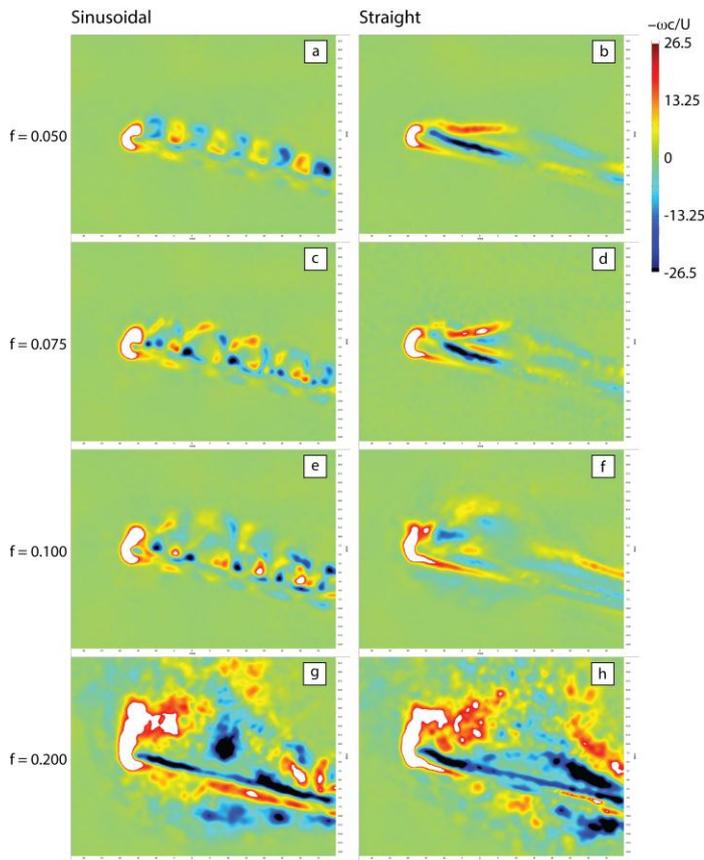
Figure 7: The vorticity plots for different flapping frequencies (f = 0.05, 0.075, 0.1, 0.2 Hz) and both straight and sinusoidal leading edge at phase angle φ = 13.3°.
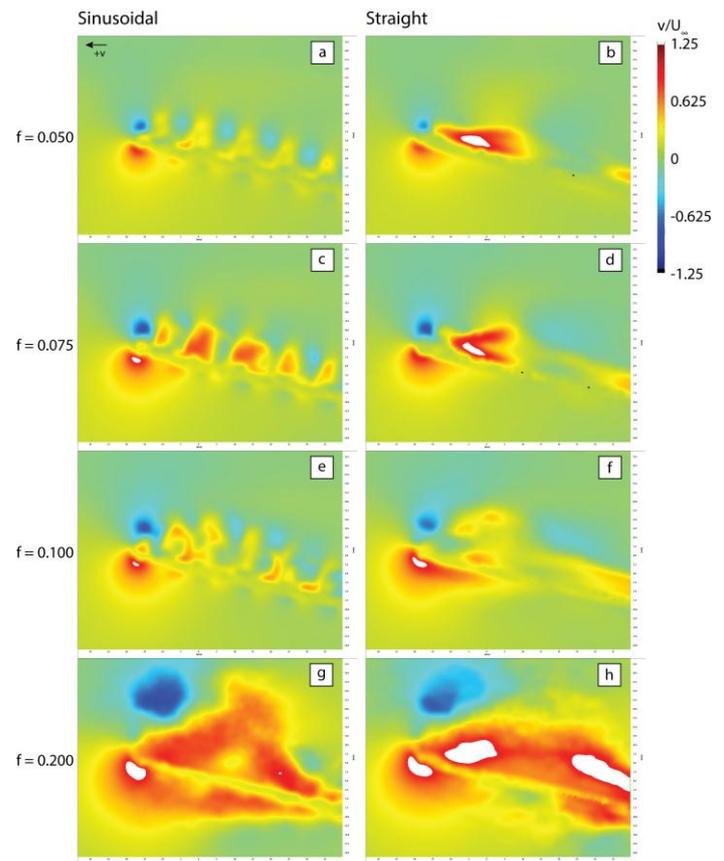
Figure 8: The spanwise flow plots for different flapping frequencies (f = 0.05, 0.075, 0.1, 0.2 Hz) and both straight and sinusoidal leading edge at phase angle φ = 13.3°.